Earth Surface Processes and Landforms

Wave Transformation Across a Macrotidal Shore Platform Under Low to Moderate Energy Conditions

Journal:	*Earth Surface Processes and Landforms*
Manuscript ID	ESP-16-0418.R3
Wiley - Manuscript type:	Research Article
Date Submitted by the Author:	n/a
Complete List of Authors:	Stephenson, Wayne; University of Otago, Department of Geography Naylor, Larissa; University of Glasgow, School of Earth and Environmental Science; Smith, Helen; University of Exeter, College of Engineering, Mathematics and Physical Sciences Chen, Bin; Guangzhou University, School of Geography Brayne, Ralph; Centre for Environment Fisheries and Aquaculture Science, Cefas
Keywords:	Shore platform, wave energy, morphodynamics, wave transformation, infragravity

Wave Transformation Across a Macrotidal Shore Platform Under Low to Moderate Energy Conditions

Wayne S.J. Stephenson[1]

Larissa A. Naylor[2]

Helen Smith[3]

Bin Chen[4]

Ralph P. Brayne[5]

[1] Department of Geography, University of Otago, PO Box 56 Dunedin, New Zealand.

[2] School of Geographical and Earth Sciences, College of Science and Engineering, University of Glasgow, University Avenue, Glasgow, G12 8QQ

[3] College of Engineering, Mathematics and Physical Sciences, College of Life and Environmental Sciences, University of Exeter, Treliever Road, Penryn, Cornwall, TR10 9EZ

[4] School of Geographical Sciences, Guangzhou University, Guangzhou 510006, China

[5] Cefas, Pakefield Road, Lowestoft, NR33 0HT, UK

Abstract

We investigate how waves are transformed across a shore platform as this is a central question in rock coast geomorphology. We present results from deployment of three pressure transducers over four days, across a sloping, wide (~200 m) cliff-backed shore platform in a macrotidal setting, in South Wales, United Kingdom. Cross shore variations in wave heights were evident under the predominantly low to moderate (significant wave height < 1.4 m) energy conditions measured. At the outer transducer 50 m from the seaward edge of the platform (163 m from the cliff) high tide water depths were 8+ m meaning that waves crossed the shore platform without breaking. At the mid platform position water depth was 5 m. Water depth at the inner transducer (6 m from the cliff platform junction) at high tide was 1.4 m. This shallow water depth forced wave breaking, thereby limiting wave heights on the inner platform. Maximum wave height at the middle and inner transducers were 2.41 and 2.39 m respectively and significant wave height 1.35 m and 1.34 m respectively. Inner platform high tide wave heights were generally larger where energy was up to 335% greater than near the seaward edge where waves were smaller. Infragravity energy was less than 13% of the total energy spectra with energy in the swell, wind and capillary frequencies accounting for 87% of the total energy. Wave transformation is thus spatially variable and is strongly modulated by platform elevation and the tidal range. While shore platforms in microtidal environments have been shown to be highly dissipative, in this macro-tidal setting up to 90% of the offshore wave energy reached the landward cliff at high tide, so that the shore platform cliff is much more reflective.

Key Words

Shore platform, wave energy, wave transformation, infragravity, morphodynamics

Introduction

Shore platforms are a conspicuous feature of rock coasts and are also found in lakes (Allan *et al*., 2002; Trenhaile, 2004) and estuaries (Kennedy, 2010). Many questions over the formation of shore platforms and likely future impacts of climate change remain unanswered (Naylor *et al*., 2010; Trenhaile, 2011, 2014a). The evolution of shore platforms is complicated by variable geological settings (geology, lithology, and tectonics), long development times (> 1000 years) and sea level changes where evolution over several glacial cycles is possible (Trenhaile 2014b). Consequently the age and rates of development of shore platforms and rock coasts is difficult to resolve; although recent modelling and the application of cosmogenic dating is improving this understanding (e.g. Choi *et al*., 2012; Thébaudeau, *et al*., 2013; Hurst et al., 2016). A holistic understanding of rock coast evolution is essential if we want to predict the resilience and vulnerability of rock coasts under changing climatic conditions.

Understanding wave transformation across shore platforms and its role in rock coast erosion is crucial to understanding the processes driving rock coast evolution. Field monitoring of wave hydrodynamics on shore platforms has been recently advanced by a number of studies investigating cross shore wave transformation and patterns of infragravity energy (f< 0.05 Hz) on platforms (Stephenson and Kirk, 2000; Taylor,

2003; Farrell *et al*., 2009; Marshall and Stephenson, 2011; Ogawa *et al*., 2011; Beetham and Kench, 2011; Ogawa *et al*., 2012; Ogawa, 2013; Ogawa *et al*., 2015; Ogawa et al., 2016; Brayne, 2016). To date, all of these instrumented studies of wave transformation on shore platforms have occurred in micro- and mesotidal (hereafter, microtidal) environments. Ogawa (2013) reported on how wave energy is expended across a mesotidal shore platform. He reported a high degree of energy dissipation across the platform and development of infragravity energy at the inner platform. Only Trenhaile and Kanyaya (2007), Poate et al. 2016 and Brayne (2016) have measured waves on platforms in macrotidal settings, however these studies did not investigate energy in the infragravity frequency. Studies in microtidal settings have revealed a variety of surf zone types including highly dissipative shore platforms (Stephenson and Kirk, 2000; Ogawa *et al*., 2012) and reflective shore platforms mixed with dissipative morphologies (Marshall and Stephenson, 2011).

A key gap in our understanding is the fate of energy delivered to rock coasts and in turn how this energy affects erosion and sediment dynamics. One approach advocated by Stephenson and Thornton (2005); Dickson *et al*. (2007) and Stephenson (2014) has been to adopt a morphodynamic framework similar to that used in beach research. In these terms rock coast morphologies can be considered reflective (e.g. plunging cliffs), intermediate (shore platforms with elements of reflection and dissipation) and dissipative (e.g. very wide platforms in shallow water). Work carried out thus far shows how tidal range, platform width, platform gradient and consequently water depth over the platform play an important role in determining the proportion of wave energy that is reflected and dissipated (Marshall and Stephenson, 2011; Beetham and Kench, 2011: Ogawa, 2013; Earlie *et al.*, 2015; Ogawa *et al.*, 2015). In microtidal environments wide platforms are highly dissipative

while narrow platforms are reflective at high tide. For microtidal platforms shallow water depth at high tide means wave breaking dissipates significant amounts of energy before reaching the landward margin of the platform where cliff retreat occurs (Stephenson and Kirk, 2000). Here, waves are forced to break either before or at the seaward edge of the platform. In the case of a macrotidal setting, wave energy can be delivered much closer to the cliff at the back of the platform because water depths are greater at high tide. It remains to be shown how much energy from deepwater is expended at the cliff platform junction. In addition to examining the transformation of wave energy, field investigations have shown the presence of significant amounts of infragravity energy occur on dissipative microtidal platforms but we are yet to demonstrate the (expected) presence of infragravity energy on macrotidal platforms. Dickson *et al*. (2013) argued that infragravity energy is important for the continual widening of horizontal platforms in microtidal environments because infragravity energy increases water depth and allows more incident wave (0.05-0.33 Hz) energy to reach the cliff foot enhancing wave erosion of the cliff and aids seismic cliff shaking and weathering processes. They suggested that continual widening negates the traditional model of steady state equilibrium where microtidal platform widening rates decrease over time due to incident wave attenuation across the widening platform. Thus, there are still important questions requiring resolution about the presence and geomorphic role of infragravity energy on rock coasts – especially in macrotidal settings with the least wave transformation research to date.

We present an instrumented field study of wave transformation across a macrotidal shore platform. We asked:

1. How are waves and energy expended across a shore platform where tidal range is large (macrotidal)?
2. How much infragravity energy is present on a shore platform in a macrotidal environment under low to moderate wave conditions?
3. What differences (if any) are there in wave transformation patterns between this macrotidal site and the existing data on microtidal and mesotidal platforms?

Study Site

The studied shore platform – cliff system is located between Nash Point and St Donat's, Wales, in the semi-diurnal macrotidal Bristol Channel with a neap to spring tidal range of 9 – 11 m tidal range (Figure 1) due to the resonance effects in the Bristol Channel. The site is exposed to Atlantic generated storm waves exceeding 5.5 m, where mean annual significant wave height is approximately 2 to 2.5 m (Channel Coast Observatory, 2014). Shore platforms are developed in Blue Lias limestone, which is characterised by alternating thin bands of shale and thicker layers of limestone (Trueman, 1930). The platforms reach widths of up to 300 m although widths less than 200 m are more common. Platforms slope seaward at about three degrees and followi the geological dip of the Lias (Trenhaile, 1972), Platforms are backed by eroding cliffs up to 30 m high and the shore platform is eroded during extreme storms (Naylor et al., 2016). The rock mass properties of the Blue Lias limestone produce a platform surface which is typically comprised of wide (200 – 300 m) smooth platform surfaces that are broken by near vertical steps between bed layers (Stephenson and Naylor, 2011).

Wave conditions in the region can be characterised using data from the Scarweather wave monitoring buoy, located approximately 40km WNW of the study site. The geographical orientation of the estuary means that waves approach the site almost exclusively from a WSW direction (Figure 2), with the distribution of significant wave height (H_s) and mean zero-crossing period (T_z) for 2009 as illustrated in Figure 2.

Methods

Field measurements

Wave measurements were made using three self-contained wave and tide recorders (RBR-2050). The instruments were factory calibrated before deployment and operate with a <1% measurement error. The three RBR-2050s were deployed along a shore normal transect where the transducers were located at the upper platform (6 m from the cliff), middle platform (90 m from the cliff) and the outer platform. The outer recorder was 163 m from the cliff and 50 m from the low tide edge of the platform (Figure 3). We assume waves cross the platform shore normal to the shore following previously published examples (e.g. Trenhaile and Kanyaya, 2007; Marshall and Stephenson, 2011; Ogawa et al., 2011, 2016); this assumption was validated using the SWAN wave model described below and accords with our observations during fieldwork . The platform profile was surveyed using a total station where elevations are reported relative to Ordnance Datum (i.e. mean sea level). In order to protect the pressure transducers from the potential impact of mobile boulders (e.g. Naylor *et al*., 2016), 65 mm diameter holes were cored into the platform surface using a petrol powered rock corer. The resistant nature of the

limestone beds of the Blue Lias meant that the time to taken to core these holes (over an hour each) prevented locating the most seaward recorder at the absolute low tide level. Each pressure transducer was placed in the hole and weighed down using lead dive weights so that the top of the transducer was flush with the platform surface. The transducer sensors were thus at the level of the platform surface while recording. They were programmed to record 2048 samples at a frequency of 4 Hz, beginning at 10 minute intervals. This results in 8.53 minute bursts separated by 2.47 minutes with no sampling (Marshall and Stephenson, 2011). Wave measurements on the platform were made over four days (12:00 hrs 08-04-2009 to 12:00 hrs 12-04-2009) capturing eight high tides during a spring tidal sequence. The raw pressure record is converted to summary wave statistics for each burst using software that supports the RBR-2050. The supporting software also compensates for the depth decay of the pressure signal using known coefficients for different wave frequencies, the depth of deployment and water depth (Gibbons *et al* 2005). Wave energy was partitioned into four frequency bands: infragravity waves (< 0.05 Hz); swell waves (0.05–0.125 Hz); wind waves (0.125–0.33 Hz); and capillary waves (> 0.33 Hz) following Ogawa *et al.* (2011; 2012; 2013; 2015). Changes in wave height, degree of wave attenuation, and wave energy transformations on the platform were assessed from summary wave statistics and power spectral analysis conducted using Matlab® (Marshall and Stephenson, 2011).

Since our wave recorders did not measure direction of wave approach nor were we able to deploy instruments off shore of the platform, we undertook wave modelling over the deployment period using the Simulating WAves Nearshore (SWAN) model (Booij et al., 1999). A coarse grid domain, with 0.01° resolution was established over the area from 3 to 5.25° W and 50.25 to 51.75° N, using offshore

wave boundary conditions from the European Centre for Medium-range Weather Forecasting (ECMWF). The offshore boundary conditions used to drive the model are shown in Figure 2. Output from the coarse grid domain model produced boundary conditions for a high resolution (0.002°) nested grid domain covering the Bristol Channel with a boundary at 4.25° W. SWAN was run in non-stationary mode to allow a higher temporal resolution and more realistic sea state evolution. Wind conditions were provided by ECMWF, and tidal heights and currents for the nested model taken from predictions for Swansea, 27 km west of the study site. The model was run from 5-15 April 2009, producing predictions for significant wave height, H_s, mean zero-crossing wave period, T_z, and direction at 30 minute intervals. The mean zero-crossing period parameter T_z was used in preference to the mean period parameter T_m to align with the data available from the wave monitoring buoys detailed below.. The actual model output point is located approximately 1 km offshore from the platform study site (Figure 1) to avoid modelling inaccuracies associated with very shallow water at low tides. The model therefore generates wave statistics at the study site before, during and after our field deployment (after Naylor et al., 2016). The predicted sea states are a statistical representation of each 30 minute period, consequently there will be a significant number of larger individual waves within each period.

Finally we supplemented our measured and modelled wave results with data from the two nearest wave monitoring sites. The first, the Minehead buoy, which is maintained by the Channel Coast Observatory (CCO, 2014) and is located at 10 m water depth offshore from Minehead, on the opposite side of the Bristol Chanel, approximately 18 km from our study site. The second is the Scarweather buoy, part of the Cefas WaveNet network of wave monitoring buoys (Cefas, 2016), located

approximately 40 km WNW of our study site at 35 m depth (Figure 1). Data from both buoys are used to provide a broader environmental context for our measured and modelled wave data, however, they are too close to the study site to provide boundary data for the SWAN model. Data from the buoys are summarised in Figure 2 .

Results

Offshore Wave Measurements Wave data for March and April 2009 from the Bristol Channel are presented in Figure 2. Data from the Scarweather buoy provide a better indication of the conditions at the platform because the buoy is fully exposed to the southwesterly seas which impact on the study site, whereas the Minehead buoy is in a more sheltered location. However, only significant wave heights and not maximum wave heights are available for Scarweather; therefore a combination of both the Minehead and Scarweather buoys were used to compare against our platform wave data. A comparison of scatter plots for Scarweather buoy data for 2009 and the platform deployment period (Figure 2) confirms that the significant wave heights experienced during the deployment are in line with the typical values seen across the year. However, the wave periods during the deployment period are notably higher than the average. Therefore although the wave energy levels experienced during the deployment can be considered typical (since energy is proportional to H_s^2), the waves are more powerful than average (with wave power additionally proportional to the wave period), with potential effects on breaking characteristics. Overall, we can characterise the deployment period as having low to moderate energy levels (with H_s in the range of 0.45 - 3.04m) relative to storm

significant wave heights that can exceed 5.6 m in the Bristol Channel (CCO, 2014). Whilst it would have been desirable to measure a wider range of energy conditions, limited field deployment time restricted the opportunity to capture a full range of wave conditions. Consequently, our analysis is limited to eight high tides over 4 days/96 hours during low to moderate energy conditions, which are similar to those measured in previous studies (Table 3). .

Offshore Modelled Waves

Figure 4 illustrates SWAN output and is compared to the seaward wave recorded on the shore platform study site. Modelled wave heights ranged from 1.09 m just before the deployment to 0.32 m just after the study period, and are strongly influenced by the tidal elevation in the region. During the transducer deployment offshore wave heights decreased. Modelled wave direction was typically between 240 and 250 deg, i.e. from a WSW direction. This is in contrast to the wave directions of approximately 250-270 degrees seen at the Scarweather buoy (Figure 3), illustrating the refraction that the waves are subject to as they approach the platform which leads to wave fronts breaking almost parallel to the cliff at high tide. The modelled wave conditions can be characterised as low energy compared with those recorded at the Scarweather buoy due to energy losses from nearshore interactions. In comparison to waves recorded on the outer edge of the platform, modelled wave heights were smaller, likely reflecting shoaling transformation of wave height as waves enter shallower water.

Incident Waves

Water level and wave heights (H_{sig} and H_{max}) over the eight tides of the deployment are displayed in Figure 5. Where data gaps occur these are during low tides when the instruments were exposed. Over the period of deployment H_{sig} ranged from 1 to 1.43 m and H_{max} did not exceed 2.41 m (Table 4). This represents non-storm conditions.

At all recorders, over the entire deployment interval, the mean significant wave period was nine seconds but ranged from 3.2 to 13 s. This wide range of wave periods results from the occurrence of both wind and swell waves during the deployment, with short period wind waves dominating the early and later part of the wave record as the tide floods and ebbs over the platform (Figure. 5). Swell waves generally dominated the middle of the wave record over each high tide, particularly on the middle and outer part of the platform. Figure 6 illustrates a representative example of one burst of data (8.5 minutes) from each of the three transducers at the same time; wave groups are evident and can be clearly seen at the middle and outer transducers.

Wave Transformation

The cross shore pattern of wave height (H_{sig}) is illustrated in Figure 7. At the peak of the high tide the largest significant (H_{sig}) waves occurred across the inner platform on seven of the eight high tides. Thus wave height tends to increase across the platform as waves shoal and rise prior to breaking. However there was one

exception to this pattern, on 9 April, when a single H_{max} wave recorded at the middle transducer was measured at 2.41 m, 2 cm larger than the 2.39 m H_{max} wave recoded at the inner platform position in a synchronous burst. On two of the high tides waves were of a similar height at all three recorders. Notably at high tide there was not a pattern of decreasing wave heights across the platform; this is the opposite of what is commonly found on microtidal shore platforms (Marshall and Stephenson 2011; Ogawa et al. 2016). This has important implications for the capacity of waves to initiate rocky shore erosion (see discussion below). These data also show a strong link between shore platform elevation and wave breaking, as breaking occurs during high tide at the highest platform elevation in the cross shore gradient (Figure 3). The same observation was made by Brayne (2016). Figure 8 illustrates wave energy on the upper platform compared to the wave energy at the middle and outer recorders over the instrument deployment. There is a general pattern of higher energy on the inner platform: wave energy is 300% and 335% greater compared with the outer platform and the middle platform, respectively.

A representative sample of power spectral density (PSD) plots are presented in Figure 9. In this figure synchronous 8.53 minute bursts are plotted from three days for two high tides and one mid tide situation. The arrows on Figure 5 (outer recorder panel) indicate the timing of these three bursts. Figure 9 show PSD at a high tide on the 8 and 9 April 2009 and at mid tide on 10 April 2009. On 8 April the PSD plots are dominated by energy in the swell and wind wave frequencies. On the middle and outer platform there is a dominance of swell (74% and 79% respectively), and wind waves account for 25% and 20% of the energy respectively. Infragravity energy is 1.3% at the middle transducer and less than 1% at the outer transducer. On the upper platform the transducer recorded more infra-gravity (i.e. 12.2% to 13.4% of the

total energy) but there is still a dominance of energy in the wind and swell frequencies.

The pattern of energy spectra over the whole field campaign is illustrated in Figure 10. The dominance of swell wave frequencies (around 0.1 Hz) is notable where most energy is in the swell frequency band. Infragravity energy is noticeably absent from the outer and middle platform, except for the small "tail" (see circle on lower panel of Figure 10. as an example) as the tide rises across the platform. On the upper recorder more infragravity energy is evident at high tide. These patterns are indicative of the low energy conditions measured.

Discussion

Our results clearly show that under low to moderate energy conditions wave characteristics across this macrotidal shore platform are tidally modulated and are influenced by variations in platform elevation. This result is consistent with previous studies in microtidal (Stephenson and Kirk, 2000; Marshall and Stephenson, 2011; Ogawa *et al*., 2011; Ogawa *et al*., 2012), mesotidal (Ogawa, 2013) and macrotidal (Trenhaile and Kanyaya, 2007; Brayne, 2016; Poate et al., 2016) settings. However the pattern of wave energy dissipation and reflection across the macrotidal platform measured here differs from that of previous studies.

Cross Platform Transformation

Under low to moderate energy conditions we found that similar sized or larger waves occurred on the inner platform at high tide compared to the middle and outer

platform. On the macrotidal shore platform reported here, deep water depths (~8 m) at high tide allows waves to cross the platform with relatively little change in wave height due to shoaling, where they break close to the cliff platform junction. The exact position of the high tide breaking point will depend on the ratio of wave height to water depth, which is modulated by platform elevation (Brayne, 2016). During our study, high tide wave breaking was limited to within 6 m of the cliff-platform junction (assuming H/h = 0.73). Thus the high tide surf zone is restricted to a narrow zone (e.g. 5-6% of platform width for a 1 m wave) on the inner part of the platform, where width of the surf zone is a function of water depth, platform elevation and wave height. When waves are less than 2 m at high tide, 90% of the platform is crossed by waves before breaking can occur. The surf zone occupies ~ 10% of the platform at high tide where the outer edge of the shore platform is only important around low tide when wave energy is focussed here. Using tidal inundation data (Figure. 5) we calculated that this window is approximately 30 minutes in duration on each flood and ebb tide (~ 60 minutes per tidal cycle). At high tide water depths across the much of the platform are too great for moderate waves to break and consequently there is little opportunity for waves to cause meso-scale platform erosion (cobble and boulder sized erosion products, e.g. Naylor *et al.*, 2012) and boulder transport (Naylor *et al.*, 2016). Consequently, this platform is likely to have a more reflective morphology than that of dissipative platforms, since high tide wave energy is expended in a relatively narrow zone on the upper part of the platform close to the reflective cliff (or steep boulder beaches where these occur).

While we have not measured waves during storm events, it can be expected that larger storm waves will create a wider surfzone, where the entire width of the surf zone will enlarge over the shore platform as the tides ebb and flow. Data on

platform erosion and boulder transport from Naylor et al. (2016) confirms this, as platform erosion and boulder transport occurred across the mid and upper intertidal zone during storm conditions. There will be some dissipation across the platform but it is likely far greater amounts of wave energy will be able to reach the upper part of the platform and the landward cliff than we measured under low to moderate wave climate.

Wave Height and Water Depth

Only two previous investigations of wave breaking on shore platforms have compared the surf zone wave height and water depth ratio commonly applied to beaches. Farrell *et al.* (2009) using H_{rms}, showed that the wave breaking height on a shore platform in Portugal was 42% of the water depth, which is similar for wave breaking in the surf zone of sandy beaches (Thornton and Guza, 1982). Ogawa *et al.* (2011) demonstrated H_{max} was limited to 0.7 water depth (h) and H_{sig} was 0.4 h. This relationship generally held across the platform although there was some variability on the seaward edge. Figure 11 shows the pattern of wave height and water depth across the Glamorgan platform by plotting H_{sig} and H_{max} against water depth. On the inner platform wave height is controlled by water depth (which is in turn modulated by platform elevation) with H_{sig} approximately 0.74 h. Using Pearson's correlation, the relationship is significant at 0.000. At the middle platform R^2 = 0.14 and significant at 0.000. While at the outer platform R^2 = 0.13 and significant at 0.000. These low R^2 values are expected given that for much of the time particularly during mid to high tide, water depths are too great to force breaking. H_{max} at the upper platform R^2 = 0.78 and is significant at 0.000. H_{max} at the mid platform site R^2 = 0.12

and is significant at 0.000. At the outer platform the R^2 value was 0.07 and also significant at 0.000. Results such as these are consistent with Trenhaile and Kanyaya (2007) and the low values for the middle and outer platform are as a result of water depths being far greater than wave height over the peak of the high tide. Thus wave breaking is a function of water depth determined by the level of tidal inundation and platform elevation which was also observed by Brayne (2016) on macrotidal shore platforms. Similar to Ogawa *et al*. (2011) there is a degree of scatter around the best fit line for the inner platform wave recording site. We attribute this to the variable water depths and small wave heights.

Infragravity Energy

Our field data unsurprisingly confirms the presence of infragravity energy on a macrotidal shore platform. At high tide in microtidal settings wave breaking releases infragravity energy on the outer edge of platforms and is found across the platform increasing shorewards (Marshall and Stephenson, 2011; Beetham and Kench, 2011; Ogawa *et al.*, 2011, Ogawa *et al.*, 2012, Ogawa, 2013). On the macrotidal platform in this study, high tide wave breaking was confined to the upper part of the platform; here wave breaking occurs more as a function of water depth rather than topography. Under higher energy conditions and a wider surf zone there would be an increase in the amount of infragravity energy available across a greater width of the platform. Under low-moderate energy conditions infragravity energy was insignificant across the platform with less than 12 to 13% of the total energy reaching the upper platform being in the infragravity band compared with 85% measured by Ogawa *et al*. (2012). Taylor (2003) noted that gravity energy was “lost” to the

infragravity band on platforms on the Kaikoura Peninsula in New Zealand and so not available for geomorphic work. More recent consideration of the role of infragravity energy suggests that the energy is still able to drive geomorphic change (Dickson *et al*., 2013). Such a low percentage of energy in the infragravity band at Glamorgan does mean more energy is in the gravity wave frequency. Regardless of the types of waves, the low to moderate energy conditions measured during this study are unlikely to have much, if any, erosive consequence. Whether infragravity energy is available for meso scale (i.e. cm – m) erosion and sediment transport requires more field investigations coupling wave, erosion and transport data under higher energy conditions. While there is still much uncertainty as to the geomorphic significance of infragravity energy on rock coast erosion (Ogawa *et al*., 2011; Dickson *et al*., 2013) it appears that it has little, if any role under low-moderate energy conditions in this macrotidal setting.

Some authors have speculated that infragravity energy may facilitate platform abrasion when infragravity energy acts to re-suspend abrasive sediments (Beetham and Kench, 2011; Marshall and Stephenson, 2011; Ogawa *et al*., 2012; Ogawa, 2013). However such a scenario requires suitably sized sediment to be available. At this site loose large cobbles and fine to medium sized boulders and are the dominant sediment classes available on the platform (Naylor and Stephenson, 2010) and it is unlikely that water level changes associated with infragravity energy would be able to suspend such large sediment particles.

Comparisons to previous wave transformation research

Our findings demonstrate that wave transformation across macrotidal shore platforms has fundamental differences with those measured under similar energy

conditions on micro to mesotidal shore platforms (Table 3). Crucially, they show that macrotidal shore platforms are reflective, with narrow energy windows within which geomorphic work can take place, where wave heights are greatest at high-tide, at the cliff-platform junction. This is the opposite of what happens on microtidal platforms (Table 3). This finding has important implications for rock coast evolution models and erosion predictions for macrotidal shore platforms and associated cliffs, particularly as storminess and sea levels increase. An important consequence of the macrotidal setting is that the outer margins and seaward edge of the platform becomes hydrodynamically disconnected from the surf zone at mid to high tide and becomes part of the subtidal offshore profile. As the ebbing tide floods the platform (i.e. the surf zone moves landward) the increasing water depth over the lower to mid-tidal sections means direct wave influences are reduced and wave breaking moves landward. On microtidal platforms relatively shallow water depths at high tide (< 1.5 m) mean that the surf zone influences much more of the platform where the outer platform is still exposed to wave forces and currents that are capable of eroding the platform and transporting debris.

Conclusions

In this macrotidal setting, waves are transformed across the study platform differently to those on platforms in microtidal settings where most previous wave transformation research has taken place. Rather than a reduction in wave height across the shore platform (as is the case in microtidal settings), waves remain the same or increase in height from the outer seaward edge to the inner margin. This pattern occurs because water depth is greater than the breaking criterion for wave

heights recorded in this study, consequently wave transformation is tidally modulated. The highest wave energies were recorded at the cliff-platform junction where ~90% of the remaining platform is effectively sub-tidal at high tide. Active wave erosion of the platform is thus most likely limited to a narrow window of opportunity as the tide floods and ebbs over the platform and only when wave heights are large enough to quarry and entrain the boulder sized erosion products (Stephenson and Naylor, 2011; Naylor *et al*., 2016). Thus wave erosion of shore platforms is closely tethered to suitable energy windows which narrows and concentrates the time period when shore platforms and cliffs are likely to be eroded by waves. Further field data, including wave measurements coupled with high resolution boulder erosion and boulder transport monitoring data, are required to validate this assumption.

Acknowledgements

W Stephenson's field work was supported by Australian Research Council grant (DP0557205). A RGS-EPSRC Small Research Grant supported L.A. Naylor. We thank Helen Jones in the University of Exeter's cartographic unit for making Figure 1. Our special thanks to James Mendelsson for his enthusiastic support of our field work.

References

Allan JC, Stephenson WJ, Kirk, RM, Taylor A. 2002. Lacustrine shore platforms at Lake Waikaremoana, North Island, New Zealand. *Earth Surface Processes and Landforms* **27**: 207-220.

Beetham EP, Kench PS. 2011. Field observations of infragravity waves and their behaviour on rock shore platforms. *Earth Surface Processes and Landforms* **36**: 1872-1888.

Booij N, Ris RC, Holthuijsen LH. 1999. A third-generation wave model for coastal regions 1. Model description and validation. Journal of Geophysical Research C: Oceans, 104(4), 7649–7666.

Brayne, R.P. 2016. The Relationship between Nearshore Wave Conditions and Coarse Clastic Beach Dynamics. Unpublished PhD Thesis, Exeter University.

Cefas, 2016. WaveNet, [online] available at: https://www.cefas.co.uk/cefas-data-hub/wavenet/ [accessed 5/9/16]

Channel Coast Observatory 2014. http://www.channelcoast.org/reports/index.php?link=&dla=download&id=550&cat=28/WaveReport2009_Mhd.pdf accessed 20-01-2014.

Choi KH, Seong YB, Jung PM, Lee SY. 2012. Using cosmogenic ^{10}Be dating to unravel the antiquity of a rocky shore platform on the West Coast of Korea. *Journal of Coastal Research* **28**: 641-657.

Dickson ME, Ogawa H, Kench PS, Hutchinson A. 2013. Sea-cliff retreat and shore platform widening: steady-state equilibrium? *Earth Surface Processes and Landforms* **38**: 1046-1048.

Dickson M, Walkden M, Hall J. 2007. Systemic impacts of climate change on an eroding coastal region over the twenty-first century. *Climatic Change* **84**: 141-166.

Earlie, CS, Young, AP, Masselink, G, Russell, PE. 2015. Coastal cliff ground motions and response to extreme storm waves. *Geophysical Research Letters* **42**(3) 846-854. doi: 10.1002/2014GL062534

Farrell EJ, Granja H, Cappietti L, Ellis JT, Li B, Sherman DJ. 2009. Wave Transformation across a rock platform, Belinho, Portugal. *Journal of Coastal Research* **SI 56**: 44–48.

Gibbons DT, Jones G, Siegel E, Hay A, Johnson F. 2005. Performance of a new submersible tide-wave recorder, in Oceans, 2005. Proceedings of MTS/IEEE, vol. 2, pp. 1057–1060, IEEE, New York.

Hurst MD, Rood DH, Ellis MA, Anderson RS, Dornbusch U. 2016. Recent acceleration in coastal cliff retreat rates on the south coast of Great Britain. *Proceedings of the National Academy of Sciences* **113**:13336-13341.

Kennedy DM, 2010. Geological control on the morphology of estuarine shore platforms: Middle Harbour, Sydney, Australia. *Geomorphology* **114**: 71 - 77.

Marshall RJE, Stephenson WJ. 2011. The morphodynamics of shore platforms in a microtidal setting: Interactions between waves and morphology. *Marine Geology* **288**: 18-31.

Naylor LA, Coombes MA, Viles HA. 2012. Reconceptualising the role of organisms in the erosion of rock coasts: A new model. *Geomorphology* **157-158:** 17-30.

Naylor LA and Stephenson WJ. 2010. On the role of discontinuities in mediating shore platform erosion. *Geomorphology* **114**: 89-100.

Naylor LA, Stephenson WJ, Trenhaile AS. 2010. Rock coast geomorphology: Recent advances and future research directions. *Geomorphology* **114**: 3-11.

Naylor LA, Stephenson WJ, Smith HC, Way O, Mendelssohn J, Cowley A. 2016. Geomorphological control on boulder transport and coastal erosion before,

during and after an extreme extra-tropical cyclone. Earth Surface Processes & Landforms. **41**: 685-700.

Naylor LA, Viles HA 2000. A temperate reef builder: an evaluation of the growth, morphology and composition of Sabellaria alveolata (L.) colonies on carbonate platforms in South Wales. Geological Society, London, Special Publications **178**: 9-19.

Ogawa H. 2013. Observation of wave transformation on a sloping type B shore platform under wind-wave and swell conditions. *Geo-Marine Letters* **33**: 1-11.

Ogawa H, Dickson ME, Kench PS. 2011. Wave transformation on a sub-horizontal shore platform, Tatapouri, North Island, New Zealand. *Continental Shelf Research* **31**: 1409-1419.

Ogawa, H, Dickson, ME, Kench, PS. 2015. Hydrodynamic constraints and storm wave characteristics on a sub-horizontal shore platform. Earth Surface Processes and Landforms **40**: 65–77.

Ogawa H, Dickson ME, Kench PS. 2016. Generalised observations of wave characteristics on near-horizontal shore platforms: Synthesis of six case studies from the North Island, New Zealand. New Zealand Geographer **50**: 107-121.

Ogawa H, Kench P, Dickson M. 2012. Field Measurements of Wave Characteristics on a Near-Horizontal Shore Platform, Mahia Peninsula, North Island, New Zealand. *Geographical Research* **50**: 179-192.

Poate TG, Masselink G, Austin MA, Dickson ME, Kench P.S 2016. Observations of Wave Transformation and Macro-tidal Rocky Platforms. *Journal of Coastal Research* SI **75**: 602-606.

Stephenson W. 2014. Rock coasts. In Masselink, G and Gehrels, R. (Eds.), *Coastal environments & global change*. (pp. 356-379). Chichester, UK: Wiley.

Stephenson WJ, Kirk RM. 2000. Development of shore platforms on Kaikoura Peninsula, South Island, New Zealand: Part One: The role of waves. *Geomorphology* **32**: 21-41.

Stephenson WJ, Naylor LA. 2011. Geological controls on boulder production in a rock coast setting: Insights from South Wales, UK. *Marine Geology* **283**: 12-24.

Stephenson WJ, Thornton LE. 2005. Australian Rock Coasts: review and prospects. *Australian Geographer* **36**: 95-115.

Taylor AJ. 2003. Change and processes of change on shore platforms. PhD Thesis, University of Canterbury, Christchurch. 386 pp.

Thébaudeau B, Trenhaile AS, Edwards RJ. 2013. Modelling the development of rocky shoreline profiles along the northern coast of Ireland, *Geomorphology* **203**: 66-78.

Thornton EB, Guza RT. 1982. Energy saturation and phase speeds measured on a natural beach. *Journal of Geophysical Research* **87(C12)**: 9499.

Trenhaile AS. 1972. Shore Platforms of Vale of Glamorgan, Wales. *Transactions of the Institute of British Geographers* 127-144.

Trenhaile AS. 2002. Rock coasts, with particular emphasis on shore platforms. *Geomorphology* **48**: 7-22.

Trenhaile AS 2004. Lacustrine shore platforms in southwestern Ontario, Canada. Zeitscrift für Geomorphology **48**: 441-59.

Trenhaile AS. 2011 Predicting the response of hard and soft rock coasts to changes in sea level and wave height. Climatic Change **109**: 599-615.

Trenhaile AS 2014a. Climate change and the impact on rocky coasts. In Kennedy DA, Stephenson WJ, Naylor LA. (eds), *Rock Coast Geomorphology: A Global Synthesis*. Memoir 40, Geological Society Books, London, 7-17.

Trenhaile AS. 2014b. Modelling the effect of Pliocene-Quaternary changes in sea level on stable and tectonically active land masses. *Earth Surface Processes and Landforms* 39: 1221-1235.

Trenhaile AS, Kanyaya JI. 2007. The role of wave erosion on sloping and horizontal shore platforms in macro- and mesotidal environments. *Journal of Coastal Research* **23**: 298-309.

Trueman AE. 1930. The Lower Lias (Bucklandii Zone) of Nash Point, Glamorgan. *Proceedings of the Geologists Association* **41**: 148–159.

LIST OF FIGURES AND TABLES

Figure 1. Location of study site and wave array across a sloping macrotidal shore platform on the Glamorgan coast, Wales, UK. Note SWAN model output located 1 km from the low tide edge of the shore platform.

Figure 2. Wave data from Minehead and Scarweather Buoys march to April 2009. Box indicates period of deployment of wave recorders on the study shore platform.

Figure 3. Cross shore profile of study platform showing location of the three wave recorders used in this study where platform elevation falls between stations was as follows: Inner – Middle (4.2 m), Inner – Outer (6.59 m), Middle – Outer (2.39 m).

Figure 4 Comparisons of SWAN wave height output with most seaward pressure transduce deployed on shore platform.

Figure 5. Wave heights (H_{sig} and H_{max}) and water depth across the shore platform over the wave recorder deployment period. Arrows indicate sample bursts shown in Figure 6.

Figure 6 Example of a synchronous burst samples at 12:00 hrs 08-04-2009 showing the water surface at each transducer. Wave groups are evident at the outer (c) and middle (b) wave recorders.

Figure 7. Cross platform variations in H_{sig}. Note slightly higher waves in the inner part of the platform compared to the middle and outer platform on six of the eight high tides.

Figure 8 Comparison of wave energy across the shore platform. Wave energy on the upper platform was calculated as a percentage of wave energy of the middle and outer platform.

Figure 9. Power spectral density plots at a high tide on the 8 and 9 April 2009 and at mid tide on 10 April 2009. The upper transducer was not inundated so there are no data for 10 April at this time stamp. Note the increased presence of infragravity energy on the middle and inner platform.

Figure. 10. Summary PSD plots for complete field deployment. Note wider plots for inner recorder at infragravity frequencies and thin tails of infragravity energy at middle and outer wave recorders (example denoted by ellipses).

Figure 11. Wave heights (H_{sig} and H_{max}) plotted against water depth at each wave recorder position across the platform.

Table 1 Annual H_{sig} exceedance and annual maximum H_{sig} 2007 to 2011, Minehead wave recorder (CCO, 2014).

Table 2. Annual H_{sig} exceedance and annual maximum H_{sig} 2007 to 2011, Scarweather wave recorder (CCO, 2014).

Table 3. Synthesis of existing wave transformation data across shore platforms (H_{sig} = significant wave height; H_{max} = maximum wave height; PT = pressure transducer; ADC = Acoustic Doppler current meter; ECM = Electromagnetic current meter).

Table 4. Summary wave statistics, water level and pressure transduce locations.

Table 1.

	Annual H_{sig} exceedance* (m)						Annual Maximum (Amax) = H_{sig}		
Year	0.05%	0.50%	1%	2%	5%	10%	Date	Amax	(m)
2007	2.36	2	1.84	1.67	1.38	1.09	2-Dec-07	21:00	2.55
2008	2.7	2.17	2.01	1.78	1.5	1.27	10-Mar-08	23:00	2.77
2009	2.13	1.81	1.65	1.5	1.23	1.02	14-Nov-09	16:30	2.53
2010	2.36	1.66	1.47	1.29	1.03	0.84	31-Mar-10	10:00	2.68
2011	2.33	1.98	1.85	1.66	1.36	1.12	15-Dec-11	4:30	2.51

Table 2

	Annual H_{sig} exceedance (m)						Annual Maximum (Amax) = H_{sig}		
Year	0.05%	0.50%	1%	2%	5%	10%	Date		Amax (m)
2007	5.12	4.25	3.83	3.46	2.98	2.45	11-Jan-07	11:00	5.49
2008	4.89	3.8	3.53	3.28	2.82	2.41	10-Mar-08	20:00	5.43
2009[1]	4.72	3.8	3.53	3.16	2.82	2.32	14-Nov-09	11:30	4.89
2010[1]	5.26	3.08	2.80	2.53	2.16	1.77	11-Nov-10	23:00	5.61
2011	4.40	3.69	3.47	3.23	2.80	2.41	15-Dec-11	03:00	4.79

[1]There is a gap in the dataset from 27/11/09 – 31/3/10. Note that data from 2007 and 2010-11 are post-processed following download from the buoy and quality control procedures, and are of a higher quality than the telemetry data used for 2008 and 2009. There appears to have been a problem with the post-processing which means that only telemetry data are available for the full length of these years. The telemetry data has been processed into bins of H_{sig} for transmission, hence the repeat values in the exceedance data. The accuracy is therefore slightly lower, but the trends in the data are correct. These data are sourced from the Cefas WaveNet database (https://www.cefas.co.uk/cefas-data-hub/wavenet/).

Table 3.

Author	Tidal Range	Platform width	Study Duration (hours)	H_{sig} (m)	H_{max} (m)	Location	Method	Size of Array
Stephenson and Kirk, (2000)	Micro	85-88	96	0.2-0.5	1.1	NZ	PT	4
Taylor, (2003)	Micro	85	60	0.2-0.5	0.3-0.7	NZ	ADCP ECM	1 2
Stephenson and Thornton (2005)	Micro	30	96	0.17-0.80		Australia	PT	2
Trenhaile and Kayana, (2007)	Meso Macro	100-180	96	0.25-0.85		Canada	Video camera and Poles	10 poles
Farrell *et al*. (2009)	Meso	70	40		0.92-1.14	Portugal	PT	7
Marshall and Stephenson (2011)	Micro	58 61 66 138	2×144	0-0.74		NZ & Australia	PT	3-5
Beetham and Kench (2011)	Micro	130 270	36	< 0.8		NZ	PT	5
Ogawa (2011)	Micro	250	24	0.4 – 0.6 m	0.86	NZ	PT	4
Ogawa *et al*. (2012)	Micro	140	24	0.5 – 0.6 m		NZ	PT	5
Ogawa (2013)	Meso	81	24	0.72 - 1.18		NZ	PT	5
Poate *et al*. (2016)	Macro					UK	PT	15
THIS PAPER	Macro	~200 m.	96	1.43	2.41	Wales, UK	PT	3

Table 4.

PT Location	Distance from cliff (m)	Shore Platform Elevation (m relative to MSL)	Hours of inundation over 4 days	T_{sig}	Largest H_{sig} (m)	Maximum high tide water depth (m)	Largest H_{max} at high tide	
							H_{max}	Date
Inner	6 m	5.85	26	5.0	1.43	1.55 m	2.39 m	8 April
Middle	90	1.64	52	9.0	1.35 m	5.7 m	2.41 m	9 April
Outer	163 m	-0.75	75	9.0	1.42 m	8.15 m	2.22 m	10 April

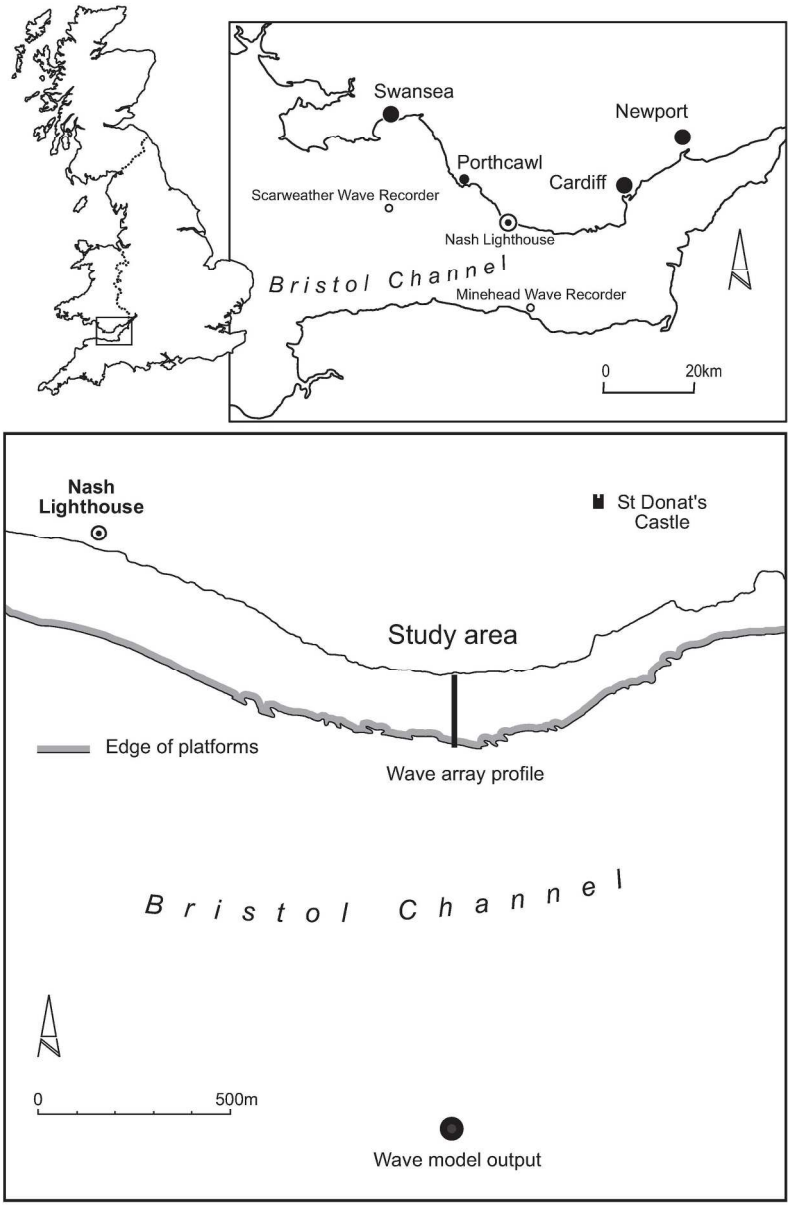

173x265mm (300 x 300 DPI)

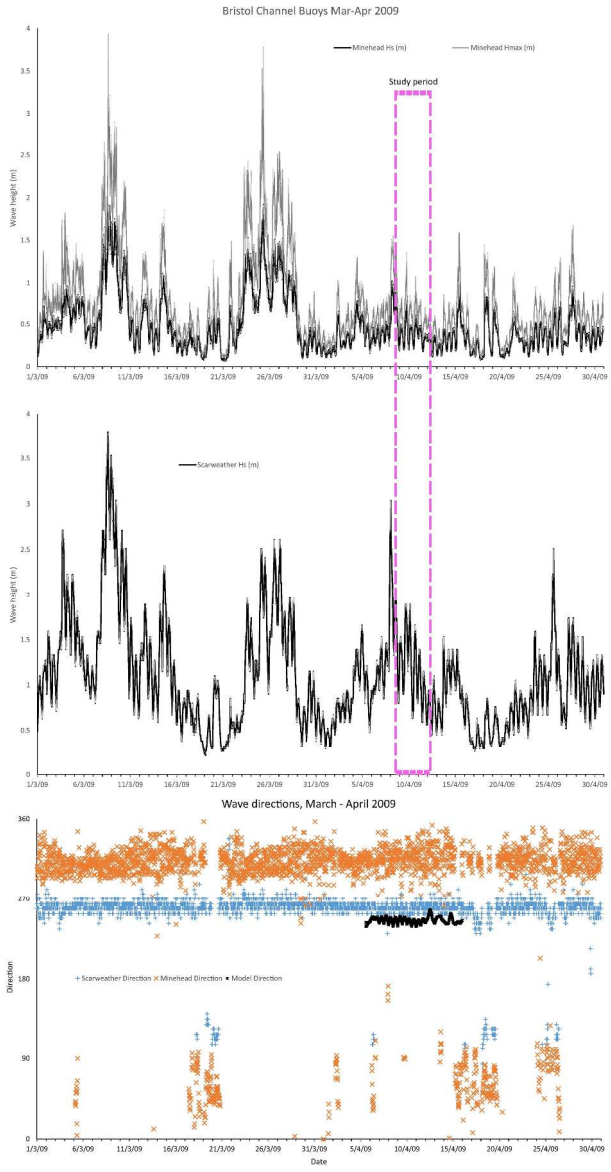

269x513mm (300 x 300 DPI)

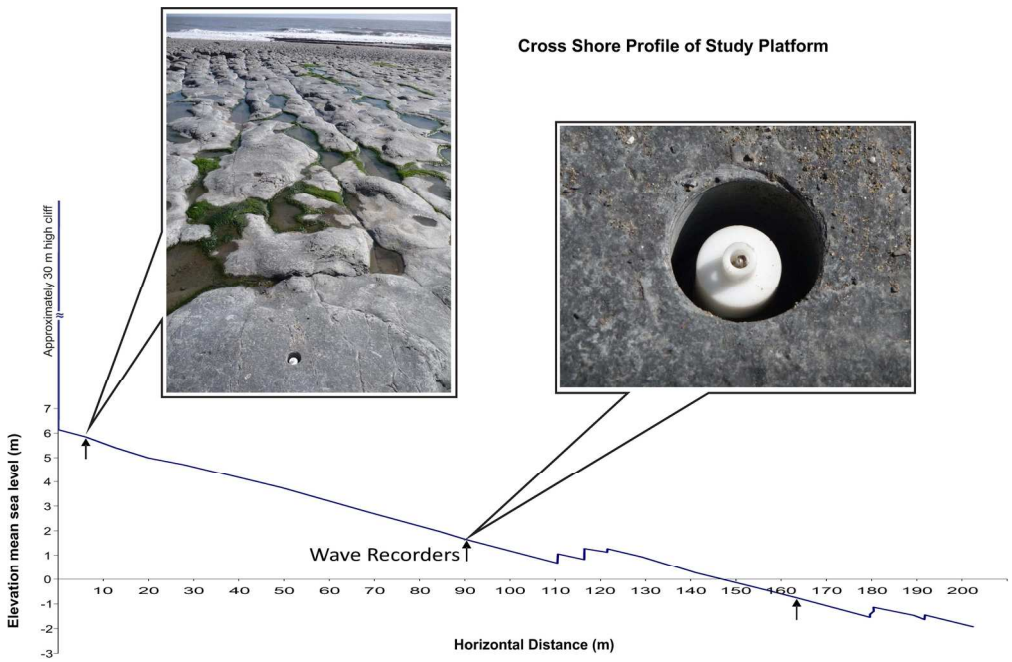

176x114mm (300 x 300 DPI)

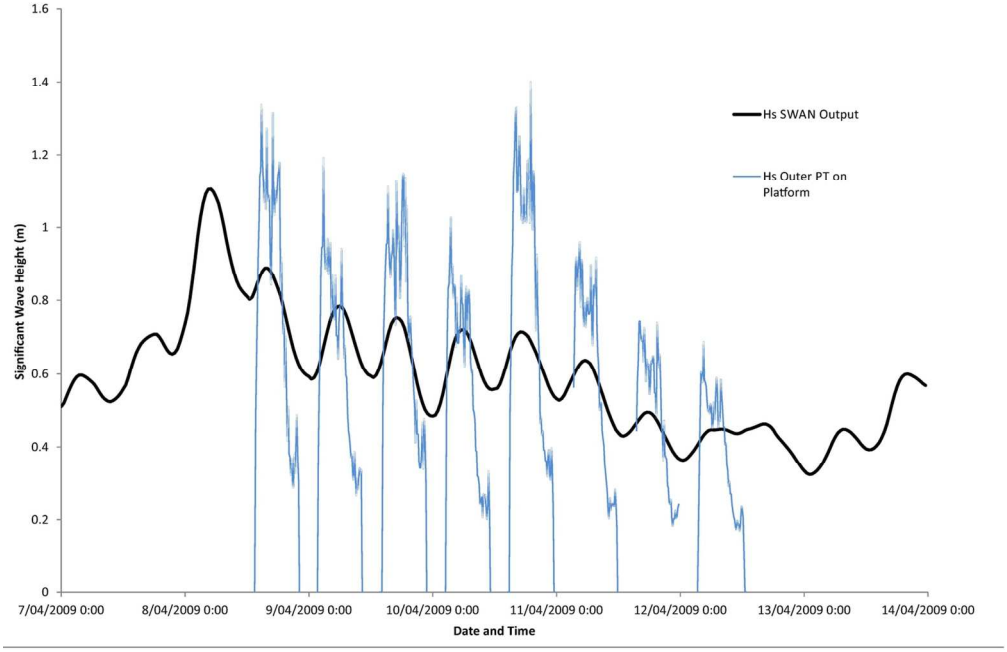

128x84mm (300 x 300 DPI)

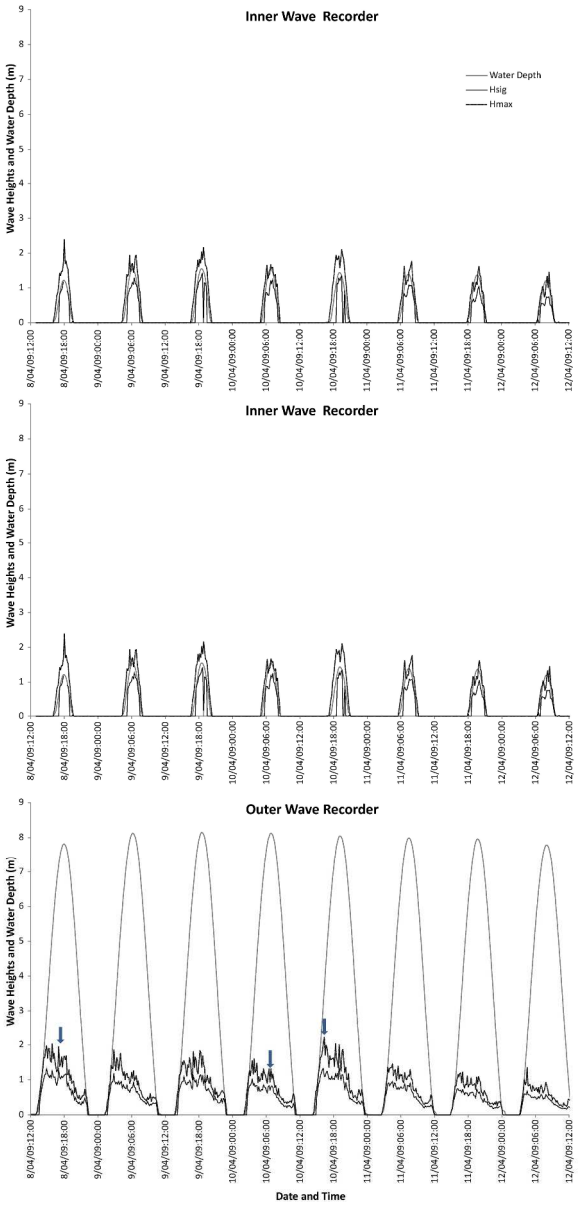

256x506mm (300 x 300 DPI)

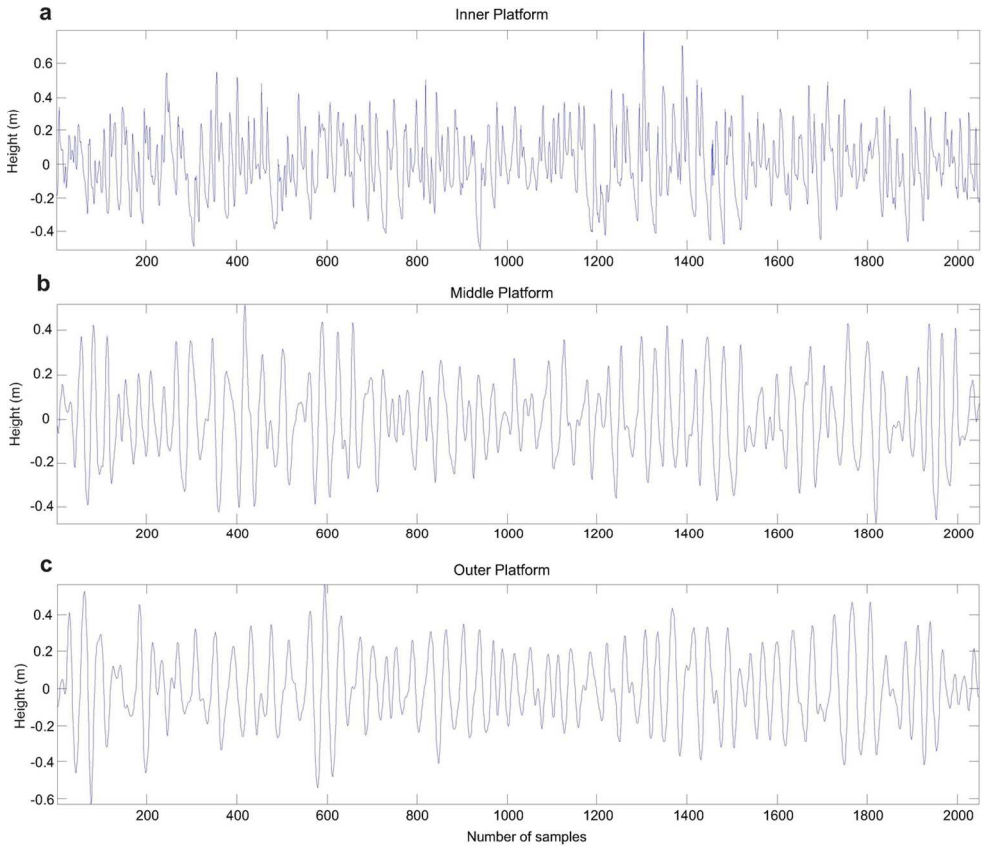

128x107mm (300 x 300 DPI)

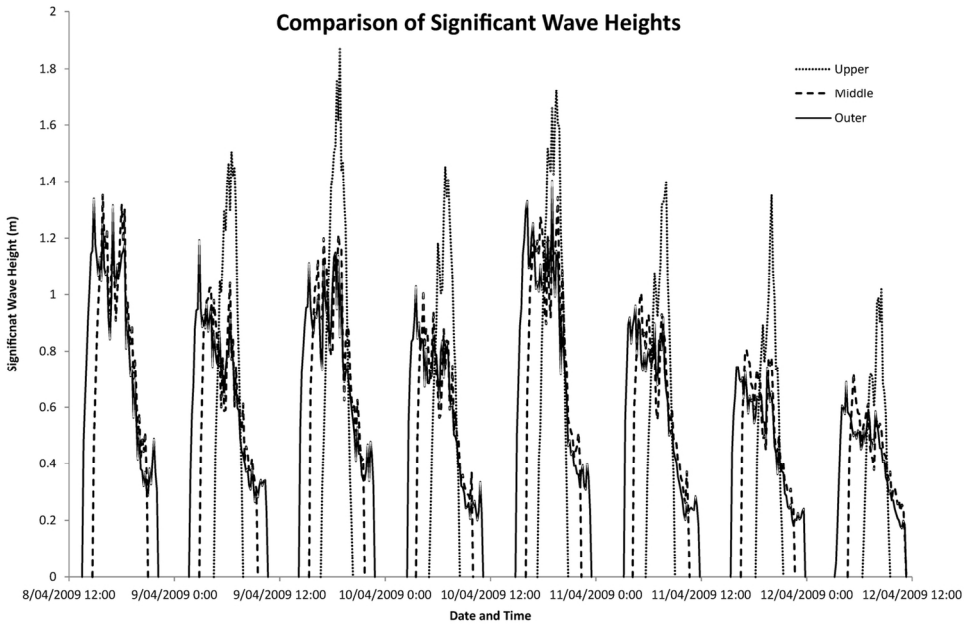

134x87mm (300 x 300 DPI)

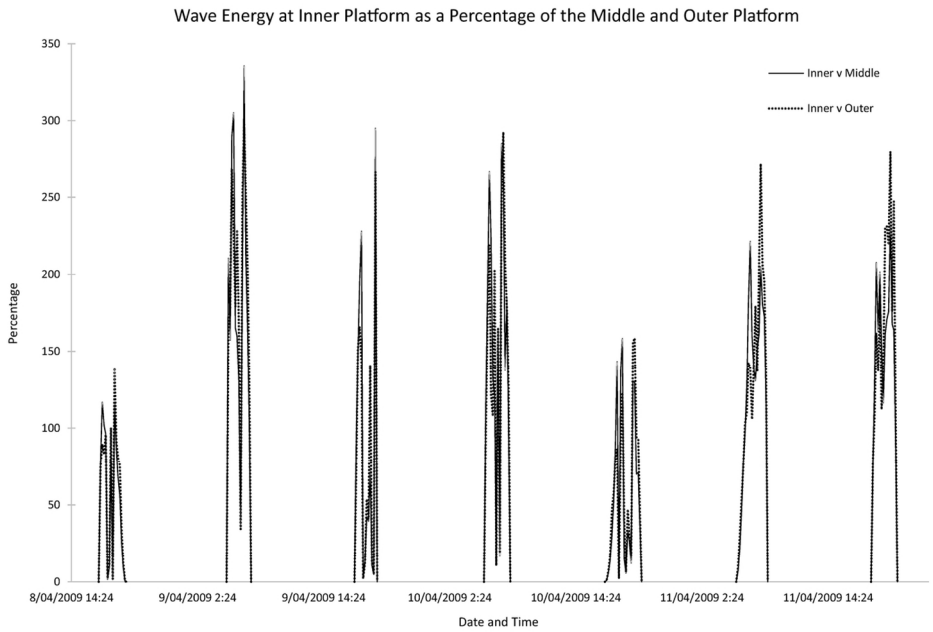

126x82mm (300 x 300 DPI)

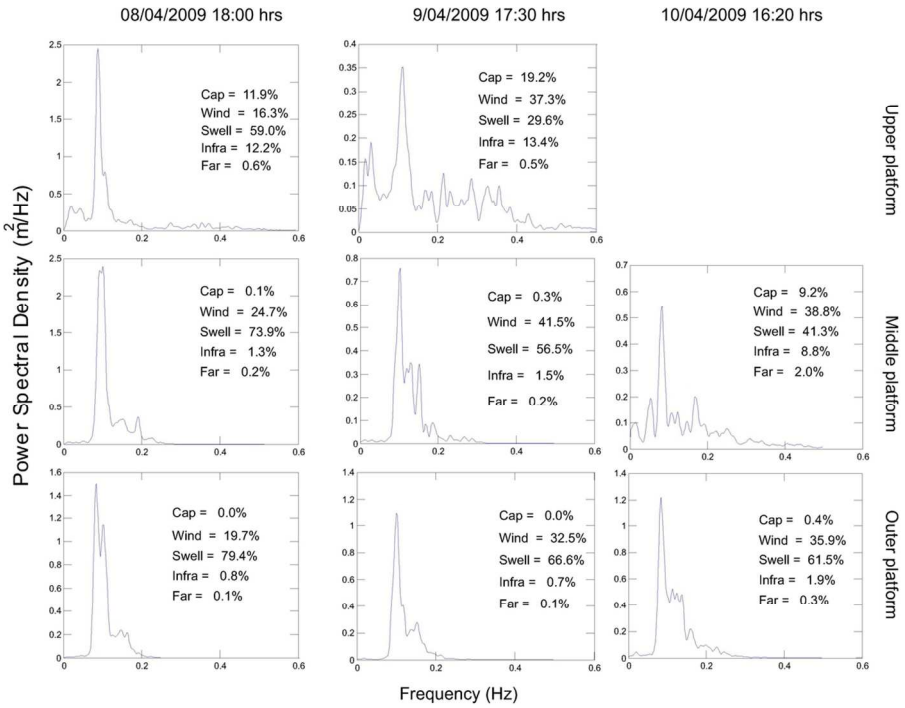

114x79mm (300 x 300 DPI)

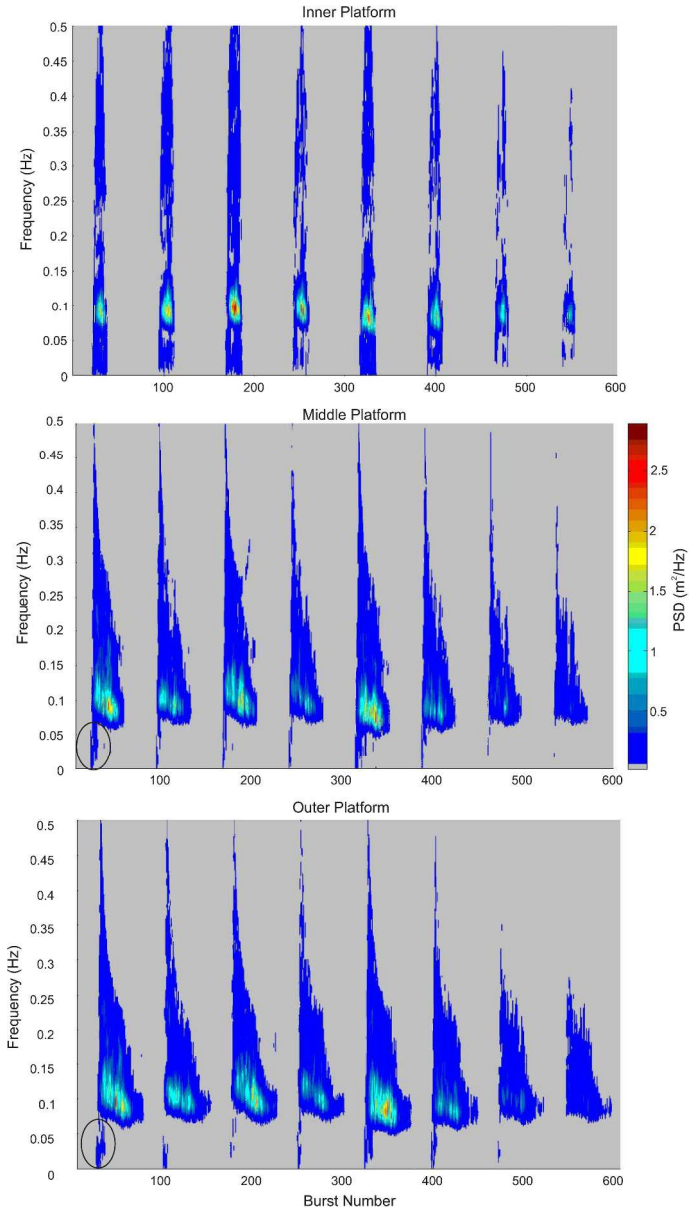

255x449mm (300 x 300 DPI)

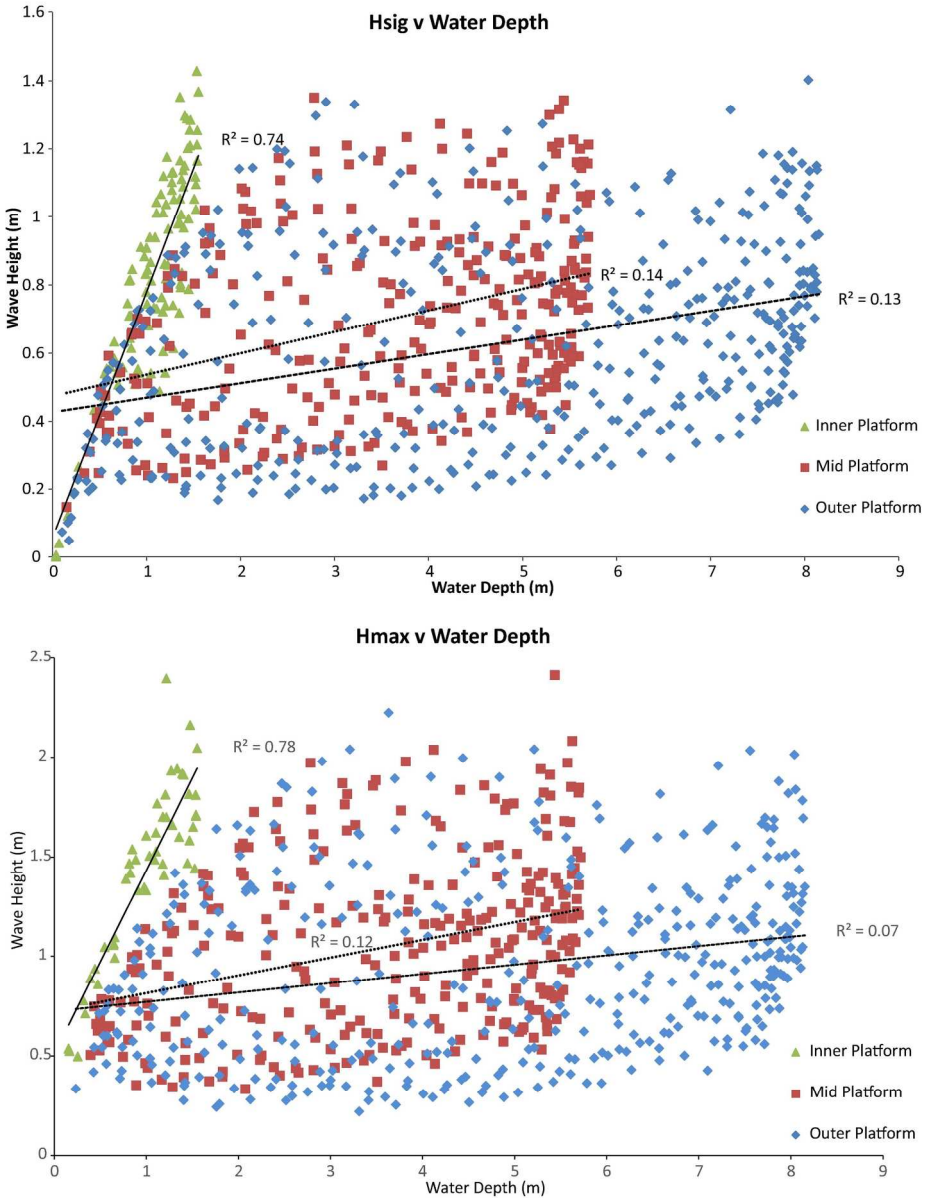

168x219mm (300 x 300 DPI)

Wave Transformation across a macrotidal shore platform under low to moderate energy conditions

Wayne J. Stephenson*, Larissa A. Naylor, Helen Smith, Bin Chen, Ralph P. Brayne.

We investigate how waves are transformed across a shore platform as this is a central question in rock coast geomorphology. In this macro-tidal setting, under the wave conditions measured, up to 90% of the offshore wave energy reached the landward cliff at high tide, so that the shore platform cliff is highly reflective. At high tide inner platform wave heights were generally larger than near the seaward edge and infragravity energy was less than 13% of the total energy spectra.